Published in final edited form as:
Circulation. 2009 August 18; 120(7): 592–599. doi:10.1161/CIRCULATIONAHA.108.813998.

Enzyme-Sensitive MR Imaging Targeting Myeloperoxidase Identifies Active Inflammation in Experimental Rabbit Atherosclerotic Plaques

John A. Ronald, Ph.D.[*,1,2,#], **John W. Chen, Ph.D., M.D.**[*,3,4,#], **Yuanxin Chen, Ph.D.**[1], **Amanda M. Hamilton, M.Sc.**[5], **Elisenda Rodriguez, Ph.D.**[4], **Fred Reynolds, Ph.D.**[4], **Robert A. Hegele, M.D.**[1], **Kem A. Rogers, Ph.D.**[5], **Manel Querol, Ph.D.**[6], **Alexei Bogdanov, Ph.D.**[6], **Ralph Weissleder, Ph.D., M.D.**[3,4], and **Brian K. Rutt, Ph.D.**[1,2,7,8]

[1]Robarts Research Institute, University of Western Ontario, 100 Perth Drive, London, ON, Canada N6A 5K8

[2]Department of Medical Biophysics, University of Western Ontario, 100 Perth Drive, London, ON, Canada N6A 5K8

[3]Center for Systems Biology, Massachusetts General Hospital, Harvard Medical School, Room 5406 CNY-149, 13th Street, Charlestown, MA 02129

[4]Center for Molecular Imaging Research, Massachusetts General Hospital, Harvard Medical School, Room 5406 CNY-149, 13th Street, Charlestown, MA 02129

[5]Department of Anatomy and Cell Biology, University of Western Ontario,100 Perth Drive, London, ON, Canada N6A 5K8

[6]Laboratory of Molecular Imaging Probes, Department of Radiology, University of Massachusetts Medical School, Worcester, MA

[7]Department of Diagnostic Radiology and Nuclear Medicine, University of Western Ontario,100 Perth Drive, London, ON, Canada N6A 5K8

[8]Department of Radiology, Stanford University, Palo Alto, California, USA

Abstract

Background—Inflammation undermines the stability of atherosclerotic plaques, rendering them susceptible to acute rupture, the cataclysmic event that underlies clinical expression of this disease. Myeloperoxidase (MPO) is a central inflammatory enzyme secreted by activated macrophages, and is involved in multiple stages of plaque destabilization and patient outcome. We report here that a unique functional *in vivo* magnetic resonance (MR) agent can visualize MPO activity in atherosclerotic plaques in a rabbit model.

#Corresponding authors: John A. Ronald, Robarts Research Institute, University of Western Ontario,100 Perth Drive, London, ON, Canada N6A 5K8, Department of Medical Biophysics, University of Western Ontario,100 Perth Drive, London, ON, Canada N6A 5K8, phone: 519-663-5777 x34316; fax: 519-663-3078; jronald@imaging.robarts.ca, John W. Chen, Center for Systems Biology, Massachusetts General Hospital, Harvard Medical School, Room 5406 CNY-149, 13th Street, Charlestown, MA 02129, Center for Molecular Imaging Research, Massachusetts General Hospital, Harvard Medical School, Room 5406 CNY-149, 13th Street, Charlestown, MA 02129, phone: 617-643-3778; fax: 617-726-5708; chenjo@helix.mgh.harvard.edu.
*JAR and JWC contributed equally

Disclosures: The authors have no disclosures.

Clinical Trial Registration Information: N/A

Methods and Results—We performed MR imaging of the thoracic aorta of New Zealand white (NZW) rabbits fed a cholesterol (n=11) or normal (n=4) diet up to 2 hours after injection of the MPO sensor bis-5HT-DTPA(Gd) (MPO(Gd)), the conventional agent, DTPA(Gd), or an MPO (Gd) analog, bis-tyr-DTPA(Gd), as controls. Delayed MPO(Gd) images (2 hour post injection) showed focal areas of increased contrast (>2-fold) in diseased wall, but not in normal wall (p=0.84), compared to both DTPA(Gd) (n=11; p<0.001) and bis-tyr-DTPA(Gd) (n=3; p<0.05). Biochemical assays confirmed that diseased wall possessed three-fold elevated MPO activity compared to normal wall (p<0.01). Areas detected by MPO(Gd) imaging co-localized and correlated with MPO-rich areas infiltrated by macrophages on histopathological evaluations (r=0.91, p<0.0001). While macrophages were the main source of MPO, not all macrophages secreted MPO, suggesting that distinct subpopulations contribute differently to atherogenesis and supporting our functional approach.

Conclusions—Our study represents a unique approach in the detection of inflammation in atherosclerotic plaques by examining macrophage function and the activity of an effector enzyme, to noninvasively provide both anatomic and functional information *in vivo*.

Keywords

magnetic resonance imaging; atherosclerosis; inflammation; myeloperoxidase; contrast media

Atherogenesis is a complex, multi-stage process that culminates in rupture of a vulnerable plaque, leading to acute arterial occlusion and life-threatening clinical end points [1, 2]. Diagnosis of atherosclerosis can occur relatively late in the disease process, just preceding or even following the occurrence of an acute event. Delayed diagnosis limits the range and application of effective evidence-based intervention strategies to reduce morbidity and mortality of atherosclerosis [3]. Therefore, there exists a pressing need to develop new biomarkers and imaging techniques to detect and evaluate vulnerable plaques prior to their rupture and to better risk stratify these patients.

Imaging inflammation has been proposed as a way to improve patient stratification and therapy monitoring since this would allow localization of inflamed plaques and the degree of inflammation in individual plaques could be tracked over time following treatment. Ultra-small superparamagnetic iron oxide nanoparticles (USPIO) or other nanoparticles have been used to detect accumulation of phagocytic cells in atherosclerotic plaques [4, 5]. However, nanoparticles may be taken up by both active and resting macrophages [6], as well as other cell types such as neutrophils, endothelial cells, lymphocytes, and smooth muscle cells [7]. In addition, different phagocytic cells play diverse roles in inflammation, with some cell types having more attenuated inflammatory or even anti-inflammatory properties [8-11]. Thus, imaging only phagocytes could overestimate the severity of plaque inflammation.

An emerging biomarker of plaque instability and future acute events is the enzyme myeloperoxidase (MPO). Elevated plasma MPO concentrations are found in stroke patients [12] and predict major downstream cardiac events both in patients presenting with acute chest pain [13], and in apparently healthy individuals [14]. Within advanced human atherosclerotic vulnerable plaques, MPO is expressed predominantly by activated macrophages and macrophage-derived foam cells [15-17] and consumes hydrogen peroxide to generate hypochlorite and other reactive oxygen species that contribute to plaque progression and rupture (Online Supplemental (OS) Fig. S1A) [18]. In this study we have examined the utility of a unique functional imaging sensor of MPO activity [19-21], called MPO(Gd), previously shown to be highly sensitive and specific to MPO activity in mouse models of multiple sclerosis [22] and myocardial infarction [23], to identify inflamed plaques in a rabbit model of atherosclerosis on a clinical magnetic resonance imaging (MRI) scanner. Our hypothesis is that once inside the diseased wall, MPO-mediated activation causes the agent to oligomerize and bind to

resident proteins, resulting in higher MR signal and prolonged retention of the activated agent within MPO-rich plaque (Fig. S1B/C).

Methods

Animal Protocol

A total of eighteen male New Zealand white (NZW) rabbits were used for this study. Eleven rabbits were fed 100 g/day of cholesterol (CH)-supplemented rabbit chow for 28-29 months to promote the formation of aortic lesions, as previously described [24, 25]. The CH level in the diet was titrated between 0.125 and 0.25% (w/w) for the length of the experiment. Please see OS text for diet details and plaque characterization (Fig. S2A). Four age-matched male NZW rabbits were used as controls and fed normal chow. Three additional CH-fed NZW rabbits (17 months on diet) were used to establish the vessel wall signal kinetics of the imaging agents. Animals were cared for in accordance with guidelines of the Canadian Council on Animal Care.

Imaging Agents

The MPO sensor, bis-5-hydroxytryptamide-diethylenetriamine-pentaacetate gadolinium (bis-5HT-DTPA(Gd) or MPO(Gd)), and the analog agent bis-tyr-DTPA(Gd) were synthesized according to a modified protocol based on Querol et al. [19]. Chemicals were purchased from Sigma-Aldrich (St. Louis, MO). DTPA-bisanhydride was reacted with serotonin (5HT) or tyramide (tyr) in dimethylformamide in the presence of an excess of triethylamine. The product bis-5HT-DTPA was isolated by recrystallization from methanol and acetone. Complexation with Gd was performed in the presence of 5% citric acid (w/w), and purified by high performance liquid chromatography. Purity of the agents was confirmed by mass spectroscopy (MALDI-TOF). DTPA(Gd) was purchased from Berlex Laboratories (Berlex, Wayne, NJ).

Magnetic Resonance Imaging

Animals were sedated via an intramuscular injection of stock anesthetic (ketamine (23.4 mg/kg), xylazine (1.3 mg/kg) and glycopyrolate (0.0075 mg/kg)) followed by intravenous administration of a 10-fold dilution (in saline) of this stock at a rate of ~3-12 ml/hr. Anesthetized rabbits were imaged in the supine position using a clinical 3T MRI scanner (GE Signa HD 12×, GE Healthcare, Waukesha, WI) interfaced with a custom-made two-channel phased array surface RF coil [25]. Axial images of the thoracic aortae of 11 CH-fed rabbits and 4 control rabbits were collected pre- and up to 2 hours post intravenous injection of either DTPA(Gd) (0.2 mmol/kg) or MPO(Gd) (0.2 mmol/kg) using a T1-weighted (T1w) quadruple inversion recovery fast-spin-echo (QIR-FSE) sequence developed previously for quantitative contrast-enhanced imaging of atherosclerotic vessels [26]. Three CH-fed rabbits were scanned up to 4 hours and at 24 hours post MPO(Gd) administration. In three additional CH-fed rabbits either MPO(Gd), DTPA(Gd), or bis-tyr-DTPA(Gd) (all at 0.1 mmol/kg) was administered and imaging was performed on a 1.5T MRI scanner (GE Signa HD 12×, GE Healthcare, Waukesha, WI). A minimum of 3 days was allowed to pass between each imaging agent administration. Finally, *ex vivo* T1w imaging was performed on perfusion fixed (10% formalin), excised aortic specimens from a CH-fed animal (17 months of feeding) sacrificed 2 hours after injection of MPO(Gd). Please see OS text for technical specifications of MRI.

MR Image and Data Analysis

MR images were analyzed with OsiriX DICOM reader (version 2.7.5, Geneva, Switzerland) by two independent readers (JR and JC). In each image, the inner and outer vessel wall boundaries were traced to determine average wall signal intensity (SI_{Wall}). Regions-of interest (ROIs) were placed in both the paraspinal muscle adjacent to the aorta and in a motion-free

region outside the animal (air) to determine average muscle signal intensity (SI_{Muscle}) and the standard deviation of the noise signal (σ_{Air}), respectively. Contrast-to-noise ratios (CNR) between the wall and adjacent muscle were calculated ($CNR = (SI_{Wall}-SI_{Muscle})/\sigma_{Air}$) and differences in CNR (ΔCNR) due to the addition of contrast agent were determined ($\Delta CNR=CNR_{2Hr}-CNR_{Baseline}$). For signal kinetics experiments, a region outside the animal was not within the field-of-view, therefore contrast ($SI_{wall}-SI_{Muscle}$) at each time point was calculated and normalized to baseline values. Enhancement ratios (ER) were determined ($ER = SI_{Wall-2Hr}/SI_{Wall-Baseline}$), as previously described [27]. ΔCNR was also calculated after tracing of select ROIs within the wall that appeared noticeably bright on images collected 2 hours after MPO(Gd) administration compared to images collected pre-contrast and 2 hours after DTPA (Gd) administration. For correlational analyses, ROIs were placed to measure plaque size and the areas positive for MPO, macrophages, lipid, and collagen in histopathological sections (see below), with the reader blinded to the other imaging results.

Histology

After imaging, animals were sacrificed with an intravenous injection of ketamine (200 mg) and transcardially-perfused under pressure with ~1.5 L of heparinized (1 IU/ml) Hanks' balanced salt solution. The imaged aortic segments were carefully isolated, marked on the ventral surface with Evan's blue dye for matching to MRI, and dissected. Fresh-frozen sections were collected from a portion (~1 mm of the 3 mm total thickness) of each block. Sections were then immunostained for plaque constituents including MPO and macrophages (RAM-11). Negative control staining was also performed. Please see OS text for tissue block preparation, additional plaque characterization (Fig. S2A) and peroxidase activity (Fig. S2B) staining, and full staining descriptions. Images of stained sections were taken using a Zeiss Axioplan 2ie microscope (Carl Zeiss Canada, Toronto, ON).

Myeloperoxidase Activity Assay

To quantify MPO activity in detergent extracts, we performed the guaiacol MPO activity assay on a Beckman Coulter DU 530 UV/vis spectrophotometer (Fullerton, CA). Briefly, the portion of each aortic block left over after sectioning (~2 mm) was homogenized in 1% cetyltrimethylammonium bromide extraction buffer followed by centrifugation for 10 minutes at 10,000 rpm. The supernatant (detergent extract) was collected and protein concentration was determined using a standardized bicinchoninic acid (BCA) assay (Pierce, Rockford, IL). The MPO activity assay solution consisted of 3 mL of 0.1 M NaPO4 buffer, supplemented with 48 ml of guaiacol and 100 μl of 0.1 M H_2O_2. To this, 25 μg of protein was added to a final volume of 0.6 ml and assayed at 25°C. The units of activity were computed according to the following formula: $Activity = (\Delta OD \times Vt \times 4)/(E \times \Delta t \times Vs)$, where ΔOD = change in absorbance; Vt = total volume; Vs = sample volume; E (extinction coefficient) = 26.6mM-1; Δt = change in time.

Statistical Analysis

A two-tailed t-test was performed for comparison between animal groups for the peroxidase activity assay (Fig. 1B). For comparisons of MR data between animal groups either a two-way repeated measures ANOVA (if normal and diseased animals were tested – Fig. 2D (both graphs)) or one-way repeated measures ANOVA were performed (Fig. 3A/B). For the above tests where multiple measurements were collected per animal (e.g., MR slices) the data was averaged to generate a single measurement per animal before performing the test. Error bars in figures represent S.E.M. Pearson correlational analysis was performed between the area of positive regions in MPO(Gd) MRI and various histological measures using data from individual plaques (Table 1). In addition, multivariable regression analysis was performed to assess the effects of both histological measures and rabbit identity (multiple plaques imaged

per rabbit) on MPO(Gd) MRI values (Table 1). The nominal level of significance for all tests was $p<0.05$. Both GraphPad Prism 4.0a (GraphPad Software Inc., San Diego, CA) and Statistical Analysis Software (SAS Institute Inc. Cary, NC) were used for statistical analysis.

Results

Hypercholesterolemic rabbits develop atherosclerotic aortic plaques that contain significant numbers of MPO-expressing macrophages

We performed MPO immunostaining on aortic sections from cholesterol (CH)-fed rabbits, and confirmed that the diseased wall expressed MPO (Fig. 1A). As in humans [17], we found that the major source of MPO in these plaques was from macrophages and macrophage-derived foam cells (Fig. 1A). Most plaques contained more macrophage-positive areas than MPO-positive areas on histopathological analysis (Fig. S3A), which matched our observation that macrophages in deeper portions of plaques expressed less MPO (Fig. 1A). MPO activity analysis in diseased aortic sections from CH-fed rabbits was more than three-fold higher than in corresponding normal aortic sections from control rabbits (Fig. 1B; $p<0.01$). Furthermore, we found moderate positive correlations between the size of individual plaques and both the area of MPO ($r=0.78$; $p<0.001$) and macrophage ($r=0.76$; $p<0.001$) immunostaining, and MPO activity ($r=0.58$; $p<0.05$) (Figs. S3B/C/D, respectively). Therefore, similar to previous findings [28], these results suggest that as MPO expression and activity increases, so does plaque size.

MPO(Gd) imaging demonstrates increased and prolonged contrast of atherosclerotic aortic wall

To understand the behavior of MPO(Gd) in diseased walls, we performed dynamic imaging following MPO(Gd) injection in three rabbits fed a CH-diet for 17 months (Fig. 2). We then compared the kinetics of the MR signal intensity change within individual plaques (compared to muscle) using MPO(Gd) with those obtained using DTPA(Gd), which has no molecular specificity (Fig. 2B). We found that both DTPA(Gd) and MPO(Gd) had similar contrast enhancement over the first 20 minutes of imaging (Fig. 2A/C), but that in certain areas of the plaques, MPO(Gd) started to demonstrate higher contrast by 30 minutes of imaging (Fig. 2C). By 2 hours an unequivocal, large difference in contrast existed between DTPA(Gd) and MPO (Gd) (Figs. 2B/C and S4A/B), and this difference persisted at nearly the same level over at least 4 hours of imaging (Fig. 2C and S4A). This is consistent with the activated agent being retained in MPO-rich regions. Furthermore, we noted that intraplaque areas that did not enhance strongly on early or late-phase DTPA(Gd) or early-phase MPO(Gd) images were clearly enhanced on delayed MPO(Gd) images (Fig. 2A/B and S4B). By 24 hours, the signal in the plaques had returned to baseline levels (Fig. S4A). Note that the same dose (0.2 mmol/kg) was administered for both agents, and that in the absence of MPO, MPO(Gd) had similar r_1 relaxivity as that of DTPA(Gd) (both approximately 4 $s^{-1}mM^{-1}$ at 1.5 T) and blood half-life (in mice, ~6 minutes) [22]. Furthermore, it was noted that the increased enhancement was often not homogeneous within the vessel wall, but was selective, showing focal areas of enhancement that persisted in the late MPO(Gd)-enhanced images but not in the late DTPA(Gd)-enhanced images (Fig. S4A).

MPO(Gd) imaging results in more than two-fold increase in contrast in areas with increased MPO activity

Based on our dynamic imaging results pre-contrast and 2-hour post-contrast imaging using MPO(Gd) and DTPA(Gd) was performed in 8 rabbits fed CH-diet for 28-29 months and 4 age-matched control rabbits. Analysis of the imaging data (Fig. 2D) revealed that in focal areas within diseased wall displaying increased signal there was more than a two-fold increase in the difference in contrast-to-noise ratio at the 2 hour time-point (ΔCNR) compared with the same regions imaged with DTPA(Gd) ($p<0.001$). In distinction, for normal wall no significant

difference in ΔCNR was noted between the two agents (p=0.84) and we also obtained similar ΔCNR values of the normal and diseased wall imaged with DTPA(Gd) (p=0.92). Representative images of normal wall after administration of either MPO(Gd) or DTPA(Gd) over the entire 2 hour period are available in OS text (Fig. S4C). To avoid potential bias, we also performed the same analysis over the entire wall (Fig. 2D). Despite averaging in areas without increased MPO activity, similar results were obtained with a 58% increase in ΔCNR between diseased and normal walls imaged with MPO(Gd) (Fig. 2D; p<0.01). Finally, enhancement ratio (ER) analysis over the entire vessel wall was performed revealing no significant difference between MPO(Gd) and DTPA(Gd) imaging for normal wall (p=0.56), whereas MPO(Gd) administration significantly and consistently enhanced diseased wall to a greater degree than DTPA(Gd) administration (p<0.0001) (Fig. S4D).

To further verify that the focal enhancement observed with MPO(Gd) imaging is not from nonspecific accumulation of MPO(Gd) but from activation by MPO, we synthesized an analog of MPO(Gd), bis-tyr-DTPA(Gd), that is a substrate for peroxidases such as horseradish peroxidase but is not activatable by MPO. We performed comparative imaging in three rabbits with MPO(Gd), bis-tyr-DTPA(Gd), and DTPA(Gd) (Fig. 3). This experiment showed that only MPO(Gd) imaging demonstrated significantly increased ΔCNR (Fig. 3A; p<0.01) and ER (Fig. 3B; p<0.01) supporting that the increased enhancement observed is the result of specific MPO activation of MPO(Gd). The bis-tyr-DTPA(Gd) non-activatable agent demonstrated an enhancement pattern and intensity similar to those of DTPA(Gd) (Fig. 3C), suggesting that the addition of small phenolic groups to a base DTPA molecule does not significantly affect distribution of an agent of this type. Furthermore, only MPO(Gd) imaging allowed the unequivocal identification of MPO rich areas that matched MPO immunohistochemistry (Fig. 3D).

MPO(Gd) imaging reveals areas of increased MPO activity in atherosclerotic plaques

To identify areas of increased MPO activity, and thus “active” inflammation, we compared MR images taken two hours after injection of MPO(Gd) with corresponding sections immunostained for MPO. Two representative sections (Fig. 4A) showed that the areas highlighted by MPO(Gd) imaging matched extremely well to MPO-positive staining. A scatter plot (Figure 4B) compared the positive areas identified on MPO(Gd) imaging to areas of positive MPO immunostaining further validated the imaging findings across all the animals studied. Multivariable regression analysis was performed to investigate any effects of rabbit identity (multiple plaques were analyzed per rabbit) and the various histological measures of plaque composition on the variability in the MR data (Table 1). This analysis revealed a significant relationship between the area of MPO immunostaining and positive MPO(Gd) (p<0.0001). No other measures achieved significance. To further validate the imaging findings, we performed correlation analysis and found that the areas highlighted during MPO(Gd) imaging at 2 hours correlated well to areas stained positive on MPO histopathology (Table 1; r=0.91; p<0.0001). We further compared MPO(Gd) imaging results to macrophage, lipid, and collagen histopathology (Table 1). We found a mild positive correlation of MPO(Gd) imaging with lipid histopathology (r=0.66; p<0.05), but no significant correlation with macrophage or collagen histopathology.

To learn about the regions of the plaque where MPO(Gd) accumulated, we also performed *ex vivo* imaging of fixed aortic segments from a rabbit sacrificed at 2 hours after MPO(Gd) administration (Fig. 5). We obtained nearly exact matches between the brightest areas in *in vivo* and *ex vivo* images. Interestingly, MPO(Gd) accumulated most often in the shoulder regions of the plaque, an area of high mechanical stress [29]. In addition, MPO(Gd) appeared to not only be retained in the intima and fibrous cap, but also penetrated into the plaque core.

Discussion

In this study, we showed that MPO activity in rabbit atherosclerotic plaques, and thus biologically relevant active inflammation, can be detected non-invasively using a clinical MR scanner by employing the MPO-activatable agent MPO(Gd). MPO rich areas are selectively enhanced by MPO(Gd) and easily identified 120 minutes post-administration. We verified that the foci of increased intensity on MPO(Gd) imaging co-localized and correlated with MPO-rich areas infiltrated by macrophages on histopathological evaluations. Biochemical assays showed that atherosclerotic plaques possessed elevated MPO activity compared to normal arterial walls, and that MPO activity correlated positively with plaque size. The results demonstrate that *in vivo* MPO activity is well associated with atherosclerotic plaque development and progression.

Our animal model develops arterial plaques that exhibit several plaque features that have been described as markers of plaque vulnerability in human plaques, including neovascularization and extensive macrophage infiltration [2, 30]. Interestingly, some areas within the plaques were rich in macrophages but not in MPO (Figs. 1 and S3), which agrees with the concept of distinct macrophage phenotypes within plaques [17]. This was supported by the strong correlation of MPO(Gd) imaging to MPO immunostaining, but not macrophage staining, since areas containing MPO-poor macrophages should not be highlighted by our agent (Table 1). There was also a mild positive correlation of MPO(Gd) imaging with lipid histopathology but not with collagen histopathology (Table 1), consistent with the concept that lipid cores are associated with more advanced unstable plaques and that many of the macrophages that produced MPO were rich in lipid (foam cells). These findings underscore the importance of our functional approach. Furthermore, the plaques in our rabbit model expressed substantially lower amounts of MPO (mean 7.7 U/mg protein) than did human atherosclerotic tissue (mean 251 U/mg protein) [16]. While underscoring some differences between rabbit and human plaques, this also has important implications for the translation of this agent for imaging human plaques, since the increased MPO content of human plaques should result in substantially greater signal intensity at sites of MPO(Gd) activation, which could allow lower doses of the agent to be used as well as increasing the sensitivity for detecting plaque vulnerability at the earliest stages of development.

Previous enzyme-sensitive MRI agents are based on a cleavage mechanism to remove masking groups that limit water access [31], albumin binding groups [32], or solubility [33]. These studies represented significant advances in imaging agent design. However, to date these prototype agents have not been shown to be effective *in vivo* without significant manipulations of the test animals (which had been limited to invertebrates and small mammals), and unlike MPO(Gd), cannot be administered intravenously, important for clinical translation. MPO(Gd) achieves signal amplification by enzymatic addition instead of cleavage. In a mouse model of myocardial infarction treated with atorvastatin, we found that MPO(Gd) was sufficiently sensitive to detect a decrease in MPO activity and inflammation [23]. Furthermore, MPO(Gd) discriminated between wild type mice with full MPO expression, MPO heterozygous mice with intermediate MPO expression, and MPO knockout mice with no MPO expression. As MPO is highly conserved across mammalian species [34], these and the results in this study confirm high sensitivity and specificity of the agent for MPO activity.

In summary, key advantages of this molecular technology lie in enabling clinical MRI scanning and T1-weighted sequences to identify pathology noninvasively and to localize and track harmful oxidative reactions in atherosclerotic lesions. An additional advantage is the short readout delay between injection and imaging (90-120 minutes). Our study provides initial proof-of-priniciple for a new, more specific imaging approach of inflammation in atherosclerosis by imaging macrophage function and the activity of an effector enzyme, and

thus is of direct biological relevance. Unlike measuring the presence of phagocytes, measuring MPO activity in plaques is likely to have greater predictive value on the risk of plaque rupture. This technology thus can localize plaques with significant active inflammation prior to devastating thromboembolic events. Consequently, it could change clinical standards by enabling earlier diagnosis and improved risk-stratification as well as allowing the ability to track the effects of timely, patient-specific interventions.

Supplementary Material

Refer to Web version on PubMed Central for supplementary material.

Acknowledgments

We thank Dr. Gloria Chiang, Allison Lee, Benjamin Bautz, Andre Belisle, Dr. Andrew Alejski, Matthew Ban, and Dr. David Sosnovik for assistance with this work.

Funding Sources: This work was funded in part by the NIH R01-HL078641 to RW and BKR, NIH 5K08HL081170 to JWC and Canadian Institutes of Health Research-Heart and Stroke Foundation of Canada (CIHR-HSFC) CMI-72324 to BKR. BKR holds the Barnett-Ivey Heart and Stroke Foundation of Ontario Research Chair. JAR holds the Great-West Life doctoral research award from the HSFC. ER is supported by the Marie Curie Fellowship.

References

1. Burke AP, Farb A, Malcom GT, Liang YH, Smialek J, Virmani R. Coronary risk factors and plaque morphology in men with coronary disease who died suddenly. N Engl J Med 1997;336(18):1276–1282. [PubMed: 9113930]
2. Virmani R, Burke AP, Kolodgie FD, Farb A. Vulnerable plaque: the pathology of unstable coronary lesions. J Interv Cardiol 2002;15(6):439–446. [PubMed: 12476646]
3. Boden WE, O'Rourke RA, Teo KK, Hartigan PM, Maron DJ, Kostuk WJ, Knudtson M, Dada M, Casperson P, Harris CL, Chaitman BR, Shaw L, Gosselin G, Nawaz S, Title LM, Gau G, Blaustein AS, Booth DC, Bates ER, Spertus JA, Berman DS, Mancini GB, Weintraub WS. Optimal medical therapy with or without PCI for stable coronary disease. N Engl J Med 2007;356(15):1503–1516. [PubMed: 17387127]
4. Kooi ME, Cappendijk VC, Cleutjens KB, Kessels AG, Kitslaar PJ, Borgers M, Frederik PM, Daemen MJ, van Engelshoven JM. Accumulation of ultrasmall superparamagnetic particles of iron oxide in human atherosclerotic plaques can be detected by in vivo magnetic resonance imaging. Circulation 2003;107(19):2453–2458. [PubMed: 12719280]
5. Hyafil F, Cornily JC, Feig JE, Gordon R, Vucic E, Amirbekian V, Fisher EA, Fuster V, Feldman LJ, Fayad ZA. Noninvasive detection of macrophages using a nanoparticulate contrast agent for computed tomography. Nat Med 2007;13(5):636–641. [PubMed: 17417649]
6. Weissleder R, Kelly K, Sun EY, Shtatland T, Josephson L. Cell-specific targeting of nanoparticles by multivalent attachment of small molecules. Nat Biotechnol 2005;23(11):1418–1423. [PubMed: 16244656]
7. Nahrendorf M, Zhang H, Hembrador S, Panizzi P, Sosnovik DE, Aikawa E, Libby P, Swirski FK, Weissleder R. Nanoparticle PET-CT imaging of macrophages in inflammatory atherosclerosis. Circulation 2008;117(3):379–387. [PubMed: 18158358]
8. Anderson CF, Mosser DM. A novel phenotype for an activated macrophage: the type 2 activated macrophage. J Leukoc Biol 2002;72(1):101–106. [PubMed: 12101268]
9. Sunderkotter C, Nikolic T, Dillon MJ, Van Rooijen N, Stehling M, Drevets DA, Leenen PJ. Subpopulations of mouse blood monocytes differ in maturation stage and inflammatory response. J Immunol 2004;172(7):4410–4417. [PubMed: 15034056]
10. Gordon S, Taylor PR. Monocyte and macrophage heterogeneity. Nature reviews 2005;5(12):953–964.
11. Nahrendorf M, Swirski FK, Aikawa E, Stangenberg L, Wurdinger T, Figueiredo JL, Libby P, Weissleder R, Pittet MJ. The healing myocardium sequentially mobilizes two monocyte subsets with

divergent and complementary functions. The Journal of experimental medicine 2007;204(12):3037–3047. [PubMed: 18025128]

12. Re G, Azzimondi G, Lanzarini C, Bassein L, Vaona I, Guarnieri C. Plasma lipoperoxidative markers in ischaemic stroke suggest brain embolism. Eur J Emerg Med 1997;4(1):5–9. [PubMed: 9152688]
13. Brennan ML, Penn MS, Van Lente F, Nambi V, Shishehbor MH, Aviles RJ, Goormastic M, Pepoy ML, McErlean ES, Topol EJ, Nissen SE, Hazen SL. Prognostic value of myeloperoxidase in patients with chest pain. N Engl J Med 2003;349(17):1595–1604. [PubMed: 14573731]
14. Meuwese MC, Stroes ES, Hazen SL, van Miert JN, Kuivenhoven JA, Schaub RG, Wareham NJ, Luben R, Kastelein JJ, Khaw KT, Boekholdt SM. Serum myeloperoxidase levels are associated with the future risk of coronary artery disease in apparently healthy individuals: the EPIC-Norfolk Prospective Population Study. J Am Coll Cardiol 2007;50(2):159–165. [PubMed: 17616301]
15. Libby P. Inflammation in atherosclerosis. Nature 2002;420(6917):868–874. [PubMed: 12490960]
16. Daugherty A, Dunn JL, Rateri DL, Heinecke JW. Myeloperoxidase, a catalyst for lipoprotein oxidation, is expressed in human atherosclerotic lesions. J Clin Invest 1994;94(1):437–444. [PubMed: 8040285]
17. Sugiyama S, Okada Y, Sukhova GK, Virmani R, Heinecke JW, Libby P. Macrophage myeloperoxidase regulation by granulocyte macrophage colony-stimulating factor in human atherosclerosis and implications in acute coronary syndromes. Am J Pathol 2001;158(3):879–891. [PubMed: 11238037]
18. Nicholls SJ, Hazen SL. Myeloperoxidase and cardiovascular disease. Arterioscler Thromb Vasc Biol 2005;25(6):1102–1111. [PubMed: 15790935]
19. Querol M, Chen JW, Weissleder R, Bogdanov A Jr. DTPA-bisamide-based MR sensor agents for peroxidase imaging. Organic letters 2005;7(9):1719–1722. [PubMed: 15844889]
20. Chen JW, Querol Sans M, Bogdanov A Jr, Weissleder R. Imaging of myeloperoxidase in mice by using novel amplifiable paramagnetic substrates. Radiology 2006;240(2):473–481. [PubMed: 16864673]
21. Querol M, Chen JW, Bogdanov AA Jr. A paramagnetic contrast agent with myeloperoxidase-sensing properties. Organic & biomolecular chemistry 2006;4(10):1887–1895. [PubMed: 16688334]
22. Chen JW, Breckwoldt MO, Aikawa E, Chiang G, Weissleder R. Myeloperoxidase-targeted imaging of active inflammatory lesions in murine experimental autoimmune encephalomyelitis. Brain 2008;131(Pt 4):1123–1133. [PubMed: 18234693]
23. Nahrendorf M, Sosnovik D, Chen JW, Panizzi P, Figueiredo JL, Aikawa E, Libby P, Swirski FK, Weissleder R. Activatable magnetic resonance imaging agent reports myeloperoxidase activity in healing infarcts and noninvasively detects the antiinflammatory effects of atorvastatin on ischemia-reperfusion injury. Circulation 2008;117(9):1153–1160. [PubMed: 18268141]
24. Daley SJ, Klemp KF, Guyton JR, Rogers KA. Cholesterol-fed and casein-fed rabbit models of atherosclerosis. Part 2: Differing morphological severity of atherogenesis despite matched plasma cholesterol levels. Arterioscler Thromb 1994;14(1):105–141. [PubMed: 8274465]
25. Ronald JA, Walcarius R, Robinson JF, Hegele RA, Rutt BK, Rogers KA. MRI of early- and late-stage arterial remodeling in a low-level cholesterol-fed rabbit model of atherosclerosis. J Magn Reson Imaging 2007;26(4):1010–1019. [PubMed: 17896368]
26. Yarnykh VL, Yuan C. T1-insensitive flow suppression using quadruple inversion-recovery. Magn Reson Med 2002;48(5):899–905. [PubMed: 12418006]
27. Sirol M, Itskovich VV, Mani V, Aguinaldo JG, Fallon JT, Misselwitz B, Weinmann HJ, Fuster V, Toussaint JF, Fayad ZA. Lipid-rich atherosclerotic plaques detected by gadofluorine-enhanced in vivo magnetic resonance imaging. Circulation 2004;109(23):2890–2896. [PubMed: 15184290]
28. McMillen TS, Heinecke JW, LeBoeuf RC. Expression of human myeloperoxidase by macrophages promotes atherosclerosis in mice. Circulation 2005;111(21):2798–2804. [PubMed: 15911707]
29. Cheng GC, Loree HM, Kamm RD, Fishbein MC, Lee RT. Distribution of circumferential stress in ruptured and stable atherosclerotic lesions. A structural analysis with histopathological correlation. Circulation 1993;87(4):1179–1187. [PubMed: 8462145]
30. Moreno PR, Purushothaman KR, Fuster V, Echeverri D, Truszczynska H, Sharma SK, Badimon JJ, O'Connor WN. Plaque neovascularization is increased in ruptured atherosclerotic lesions of human

aorta: implications for plaque vulnerability. Circulation 2004;110(14):2032–2038. [PubMed: 15451780]

31. Louie AY, Huber MM, Ahrens ET, Rothbacher U, Moats R, Jacobs RE, Fraser SE, Meade TJ. In vivo visualization of gene expression using magnetic resonance imaging. Nat Biotechnol 2000;18 (3):321–325. [PubMed: 10700150]
32. Nivorozhkin AL, Kolodziej AF, Caravan P, Greenfield MT, Lauffer RB, McMurry TJ. Enzyme-Activated Gd(3+) Magnetic Resonance Imaging Contrast Agents with a Prominent Receptor-Induced Magnetization Enhancement We thank Dr. Shrikumar Nair for helpful discussions. Angewandte Chemie (International ed 2001;40(15):2903–2906.
33. Himmelreich U, Aime S, Hieronymus T, Justicia C, Uggeri F, Zenke M, Hoehn M. A responsive MRI contrast agent to monitor functional cell status. Neuroimage 2006;32(3):1142–1149. [PubMed: 16815042]
34. Sakamaki K, Ueda T, Nagata S. The evolutionary conservation of the mammalian peroxidase genes. Cytogenetic and genome research 2002;98(1):93–95. [PubMed: 12584448]

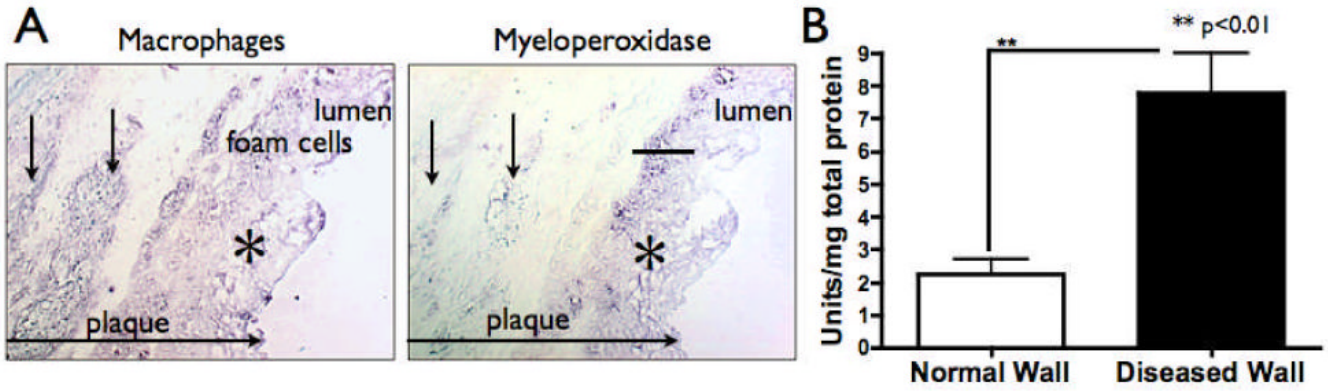

Fig. 1.

(A) RAM-11 and MPO immunostaining on adjacent sections, revealed that macrophages and macrophage-derived foam cells at the surface of plaques expressed significant amounts of MPO (*). In contrast, macrophages found in the deeper parts of the plaques often weakly expressed MPO (arrows) (scale bar represents 100 μm). **(B)** On average, MPO activity of diseased wall was 3-fold higher than in normal wall (n=8, 23 sections analyzed for diseased wall; n=4, 12 sections analyzed for normal wall).

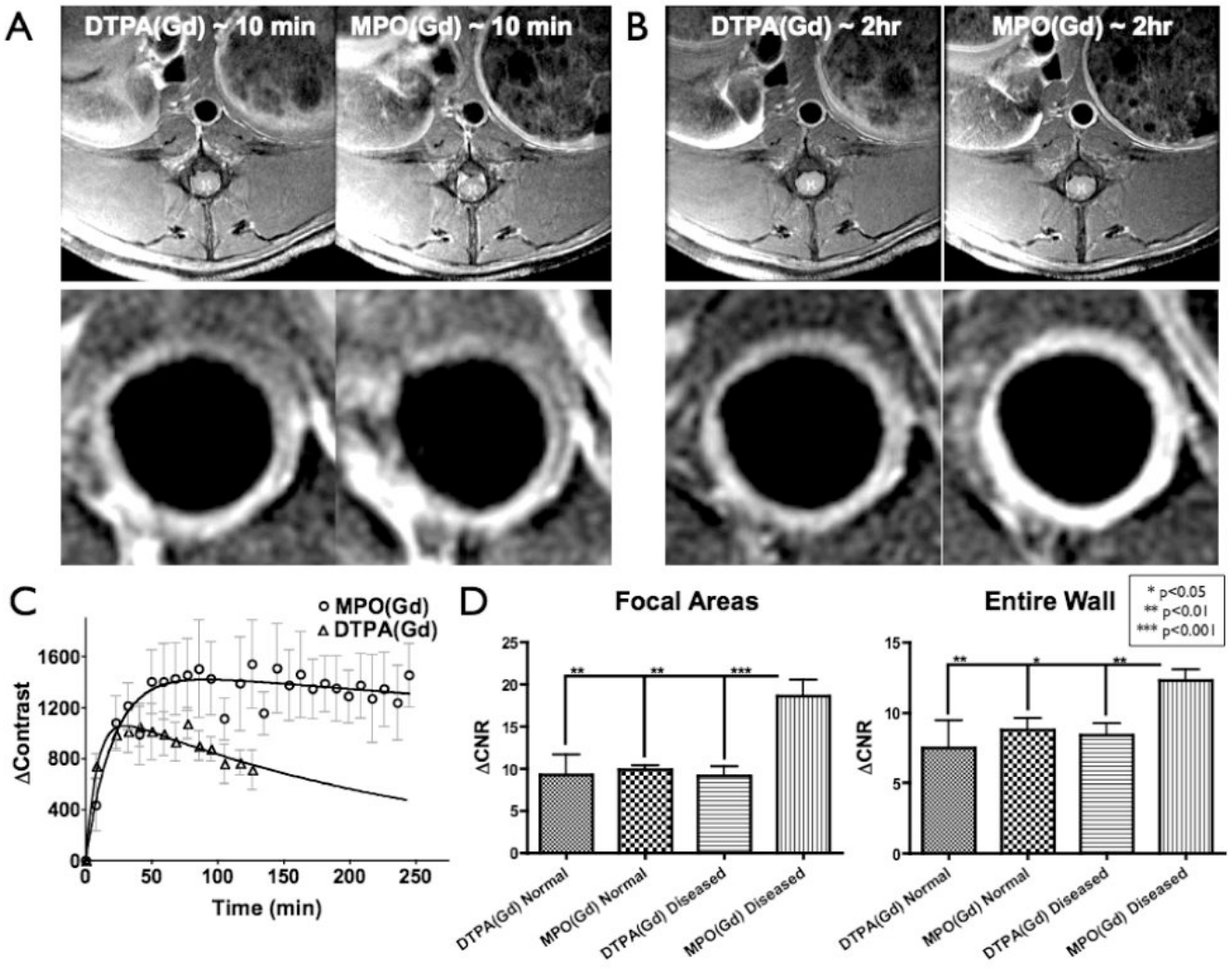

Fig. 2.

(A) As acquired (5 cm field-of-view – top) and higher magnification (bottom – centered around aorta) early-phase (~10 min.) MR images of diseased wall in rabbit fed CH-diet for 17 months using DTPA(Gd) (left) and MPO(Gd) (right). Similar levels of enhancement were seen at this time point using both agents. **(B)** Delayed MPO(Gd) images (~2 hrs - right) showed substantially increased enhancement compared to both late-phase (~2 hrs - left) and early-phase (seen in **A**) DTPA(Gd) images. **(C)** Kinetics study: Increased and prolonged contrast was found using MPO(Gd) compared to DTPA(Gd) (n=3 animals). **(D)** Analysis of pre-contrast and 2 hour post-contrast MR images of rabbits fed CH-diet for 28-29 months (n=8) and age-matched controls (n=4) using MPO(Gd) and DTPA(Gd). ΔCNR in both focal wall areas (left) and the entire wall (right) revealed no difference using MPO(Gd) and DTPA(Gd) in normal wall (n=4, 11 sections analyzed). Diseased wall imaged using DTPA(Gd) (n=8, 24 sections analyzed) also showed no difference compared to normal wall with either agent. In distinction, diseased wall imaged using MPO(Gd) (n=8, 24 sections analyzed) showed significantly higher ΔCNR (~2X) compared to all other values.

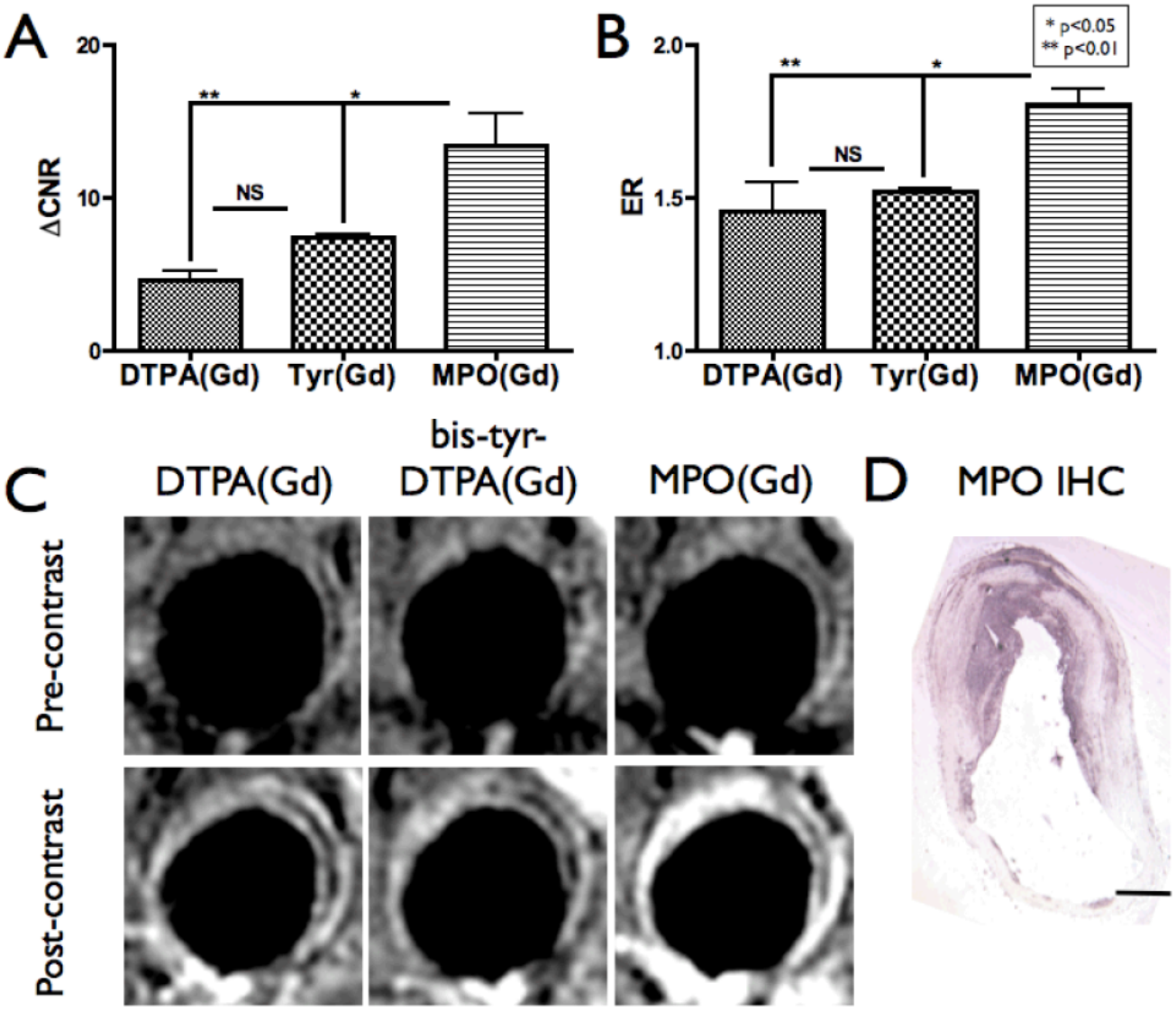

Fig. 3.

Imaging with a nonactivatable analog of MPO(Gd). **(A)** ΔCNR and **(B)** ER analysis of diseased walls in CH-fed rabbits (n=3 rabbits, 11 sections analyzed) imaged after the administration of DTPA(Gd), MPO(Gd), and a nonactivatable analog of MPO(Gd) (bis-tyr-DTPA(Gd)), with each agent administered at least 3 days apart. Significantly increased ΔCNR and ER using MPO(Gd) compared to both control agents was found, supporting that the increased enhancement observed is the result of MPO activation of MPO(Gd). No significant (NS) differences were observed between the analog and DTPA(Gd). **(C)** Representative 2 hour delayed images demonstrating that only the activatable MPO(Gd) is able to show focal increased enhancement to confirm MPO activity. The window/level settings were determined on the pre-contrast images to ensure that the paraspinal muscles appear similar between the images for each agent, and then these settings were applied to the post-contrast images. **(D)** MPO immunohistochemistry (IHC) confirms MPO(Gd) imaging findings.

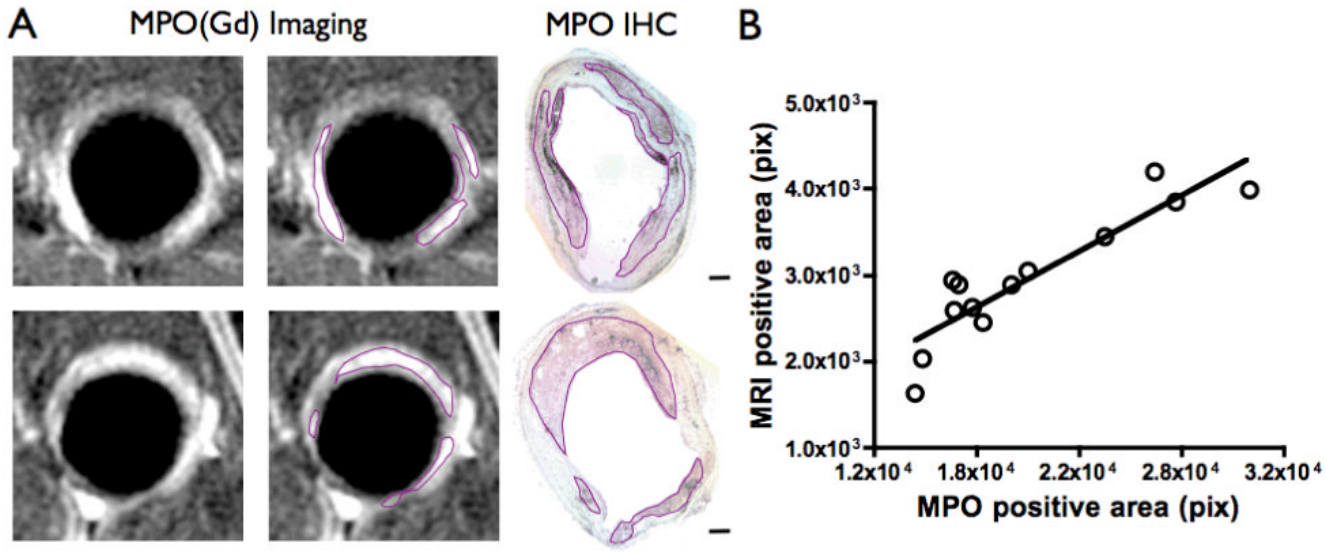

Fig. 4.

MPO(Gd) imaging identifies distinct foci of MPO activity in diseased atherosclerotic wall. **(A)** MPO(Gd) images of diseased wall taken 2 hours after administration revealed focal regions of increased enhancement. These regions correlated well with portions of the plaque identified as rich in MPO in immunostained, matched sections (scale bar=500 μm). Outlined areas on the second column of MR images are shown as a visual aid. **(B)** Scatter plot of positive areas by MPO immunostaining versus the positive areas identified by MPO(Gd) imaging (n=8 animals, 13 sections). Line represents regression line.

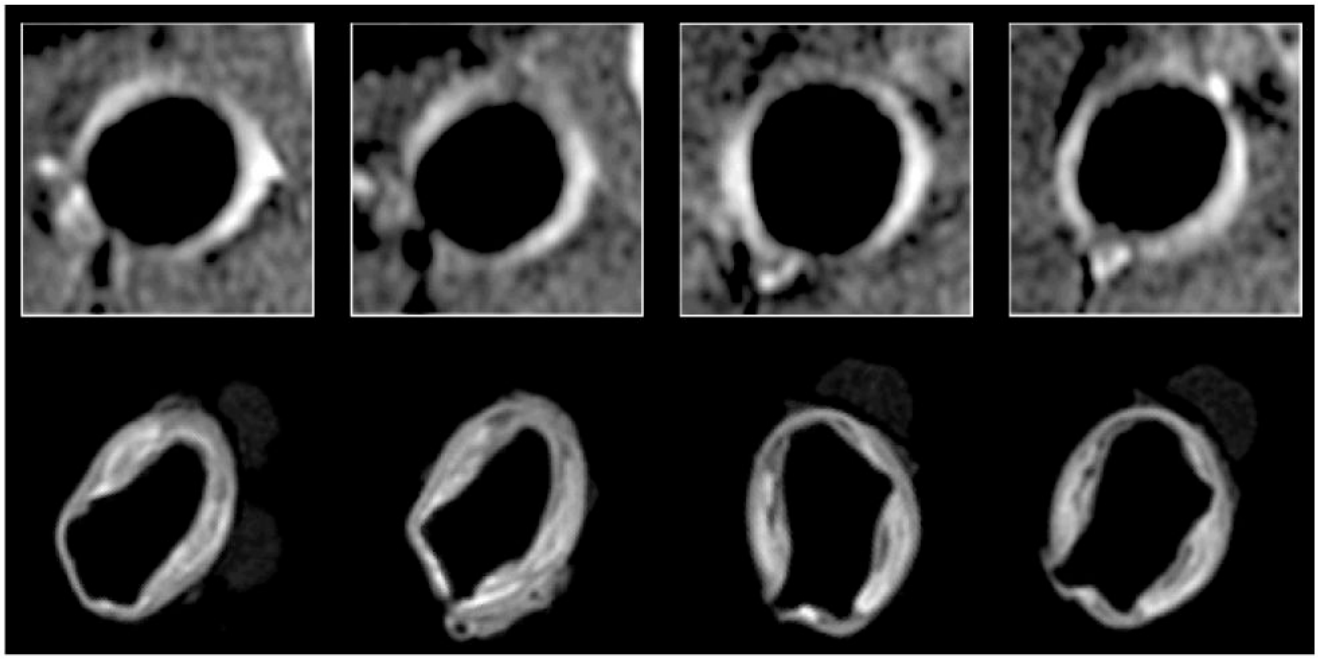

Fig. 5.
Matched *in vivo* (0.195 × 0.260 × 5 mm^3) and *ex vivo* (0.1 × 0.1 × 0.3 mm^3) images of the diseased aorta of a CH-fed rabbit 2 hours after injection of MPO(Gd). Images were aligned with the help of agarose beads adhered with cyanoacrylate to the ventral and right side of the aorta after fixation. In the 4 examples, nearly exact matches between the brightest areas *in vivo* and *ex vivo* images are noted. Interestingly, it appears that MPO(Gd) accumulated most often in the shoulder regions of the plaque and was retained not only in the intima and fibrous cap, but also penetrated into the plaque core.

Table 1

Multivariable Regression Parameters for Positive Areas of MPO(Gd) Imaging Based on Model including Rabbit Identity and Various Histological Measures of Plaque Composition

	Regression Parameters			
Independent Variable	**P-value**	**Partial R-square**	**Model R-square**	**r-value* (p-value)**
MPO IHC	<0.0001	0.82	0.82	0.91 (<0.0001)
Mac IHC	NS	…	…	NS
Lipid	NS	…	…	0.66 (<0.05)
Collagen	NS	…	…	NS
Rabbit	NS	…	…	

* Pearson correlation coefficient in analysis of histological measures to positive areas of MPO(Gd) imaging.

NS = not significant (p>0.15).